Available online at www.sciencedirect.com
ScienceDirect
Planetary and Space Science 56 (2008) 1260–1272
Planetary and Space Science
www.elsevier.com/locate/pss

Mass loss from "Hot Jupiters"—Implications for CoRoT discoveries, Part II: Long time thermal atmospheric evaporation modeling

T. Penz[a,*], N.V. Erkaev[b], Yu.N. Kulikov[c], D. Langmayr[d], H. Lammer[d], G. Micela[a], C. Cecchi-Pestellini[g], H.K. Biernat[d,e], F. Selsis[f], P. Barge[h], M. Deleuil[h], A. Léger[i]

[a]*INAF, Osservatorio Astronomico di Palermo, I-90134, Palermo, Italy*
[b]*Institute for Computational Modelling, Russian Academy of Sciences, 660036 Krasnoyarsk, 36, Russian Federation*
[c]*Polar Geophysical Institute (PGI), Russian Academy of Sciences, Khalturina Str. 15, 183010, Murmansk, Russian Federation*
[d]*Space Research Institute, Austrian Academy of Sciences, Schmiedlstr. 6, A-8042 Graz, Austria*
[e]*Institute for Physics, University of Graz, Universitätsplatz 5, A-8010 Graz, Austria*
[f]*Centre de Recherche en Astrophysique de Lyon (CRAL), and Ecole Normale Supérieure (ENS), Lyon, France*
[g]*INAF, Osservatorio Astronomico di Cagliari, Cagliari, Italy*
[h]*Observatoire d Astrophysique de Marseille, B.P. 8, F-13376 Marseille, Cedex 12, France*
[i]*Institut d' Astrophysique Spatiale, bat 121, CNRS, Univ. Paris Sud, F-91405 Orsay, France*

Received 16 June 2006; accepted 9 July 2007
Available online 3 May 2008

Abstract

We investigate the efficiency of the atmospheric mass loss due to hydrodynamic blow-off over the lifetime of the exoplanet HD209458b by studying numerically its hydrogen wind for host star X-ray and EUV (XUV) fluxes between 1 and 100 times that of the present Sun. We apply a time-dependent numerical algorithm which is able to solve the system of hydrodynamic equations straight through the transonic point of the flow including Roche lobe effects. The mass loss rates are calculated as functions of the absorbed energy in the thermosphere. Depending on the heating efficiency for a hydrogen-rich thermosphere the maximum temperature obtained in our study at $1.5R_{pl}$ by neglecting IR cooling is about 5000–10,000 K for heating efficiencies of 10% and 60%, respectively. We find that the upper atmosphere of HD209458b experiences hydrodynamic blow-off even at such low temperatures if one does not neglect gravitational effects caused by the proximity of the planet to its Roche lobe boundary. Depending on the heating efficiency, we find from the solution of the hydrodynamic equations of mass, momentum, and energy balance that energy-limited mass loss rate estimations overestimate the realistic mass loss rate at present time for HD209458b by several times. Using the maximum heating efficiency for hydrogen–rich atmospheres of 60% we find that HD209458b may experience an atmospheric mass loss rate at present time of about 3.5×10^{10} g s^{-1}. The mass loss rate evolves to higher values for higher XUV fluxes expected during the early period of the planet's host star evolution, reaching values of several times 10^{12} g s^{-1}. The integrated mass loss is found to be between 1.8% and 4.4% of the present mass of HD209458b. We found that the influence of the stellar tidal forces on atmospheric loss (the Roche lobe effect) is not significant at 0.045 AU. For a similar exoplanet, but at closer orbital distances $\leqslant$0.02 AU, the combined effect of the Roche lobe and the high XUV radiation result in much higher thermal loss rates of about 2.6×10^{11} g s^{-1} and even more for early stages. This leads to a total loss over 4 Gyr of 27.5% of the planetary mass.

Keywords: Hydrodynamic modeling; Exoplanets; Atmospheric evolution; Mass loss; Roche lobe; CoRoT

1. Introduction

The "Hot Jupiter" HD209458b which orbits around an about 4 Gyr old solar-like G star is the first exoplanet for which several transits across the stellar disk have been observed (Henry et al., 2000; Charbonneau et al., 2000) indicating that its visual radius is only slightly larger than Jupiter's, that is about $1.32r_{Jup}$ (Knutson et al., 2007; Ballester et al., 2007). After several unsuccessful attempts to observe atmospheric species of HD209458b by Bundy and Marcy (2000), Rauer et al. (2000), and Moutou et al.

*Corresponding author. Tel.: +39 091 233264; fax: +39 091 233444.
E-mail address: tpenz@astropa.inaf.it (T. Penz).

0032-0633/$ - see front matter © 2008 Elsevier Ltd. All rights reserved.
doi:10.1016/j.pss.2008.04.005

(2001), Charbonneau et al. (2002) observed a dense lower atmosphere of HD209458b and detected neutral sodium due to absorption in the NaI D lines. The spectroscopic observations of the absorption in the NaI D lines and H Lyman-α line during transits provided the first opportunity to constrain the structure of the atmosphere of a "Hot Jupiter". The size of the planet inferred from the H Lyman-α absorption corresponds to atomic hydrogen density n_H of at least $10^6\,cm^{-3}$ at a planetary distance of about $2.5r_{pl}$ (Vidal-Madjar et al., 2003). Vidal-Madjar et al. (2003) concluded from their observations that atomic hydrogen escapes from the extended upper atmosphere of HD209458b with a rate of more than $10^{10}\,g\,s^{-1}$.

Vidal-Madjar et al. (2004) analyzed four more transits of HD209458b with the space telescope imaging spectrograph (STIS) on board of the hubble space telescope (HST) in the wavelength range of 118.0–171.0 nm and found absorptions in HI, OI, and CII absorption lines. They found that the absorption over the whole HI Lyman-α line is consistent with their previous observation (Vidal-Madjar et al., 2003) and the absorption depths for OI and CII show that atomic oxygen and carbon are also present up to the Roche lobe and beyond. These results can be interpreted as an observational evidence of the existence of the upper atmosphere which experiences hydrodynamic blow-off conditions. Because of the high X-ray and EUV (XUV) flux of a close host star, the upper atmospheres of short-periodic hydrogen-rich gas giants can be heated to temperatures $\geqslant 10,000\,K$, resulting in large escape rates and intense cooling by a planetary hydrogen wind which can also drag along with it heavier atomic species-like O and C beyond the exobase or even the Roche lobe.

The theory of hydrodynamic escape of hydrogen and heavier species, dragged off along with the light species, has been developed by Hunten (1973) and applied to mass fractionation of heavy isotopes in the early atmospheres of Venus, Earth, and Mars by Zahnle and Kasting (1986), Zahnle et al. (1990), and Hunten (1993). Hydrodynamic escape consists of a global, cometary-like (Schneider et al., 1998), expansion of the upper atmosphere. These conditions occur if a large amount of the energy of the stellar XUV radiation is deposited in the thermosphere, allowing heated atoms to overcome the gravity field of a planet and to flow as a planetary wind (blow-off) into interplanetary space (Hunten, 1973, 1993; Zahnle and Kasting, 1986; Zahnle et al., 1990; Chassefière, 1996a, b; Pepin, 2000; Pepin and Porcelli, 2002; Becker et al., 2003).

Lammer et al. (2003) applied a scaling method (Bauer, 1971; Gross, 1972) for the estimation of the exospheric temperature of "Hot Jupiters" and found that T_{exo} can easily reach values $\geqslant 10,000\,K$ at orbital distances $<0.1\,AU$, if efficient cooling by IR-irradiating molecules-like H_3^+ is neglected. Yelle (2004, 2006) applied 1-D hydrodynamic calculations of the atmospheric structure of "Hot Jupiters" in orbits with semi-major axes from 0.01 to 0.1 AU and found a hydrogen loss rate of about $4.6\times10^{10}\,g\,s^{-1}$. In agreement with Lammer et al. (2003), this study showed that the thermospheres of short-periodic gas giants may be heated to temperatures up to about 10,000 K by the XUV flux from the central star alone. Observational evidence of the XUV heating within the lower thermosphere of HD209458b was recently provided by Ballester et al. (2007) who detected a 0.03% Balmer-continuum absorption. After applying the Yelle (2004) model they found that a layer of hot hydrogen with a temperature of about 5000 K can explain the observations. Tian et al. (2005) developed a numerical model which solves the time-dependent hydrodynamic equations of mass, momentum, and energy balance, by using a Chapman-like 2-D energy deposition function instead of the single layer approximation of absorbed XUV radiation of Watson et al. (1981) and applied it to HD209458b. These authors found a maximum loss rate of about $6\times10^{10}\,g\,s^{-1}$ which is in agreement with that of Yelle (2006) and about a factor of 15 less than the energy-limited loss rate estimate of about $10^{12}\,g\,s^{-1}$ obtained by Lammer et al. (2003) who used the energy-limited equation and the single XUV layer approximation of Watson et al. (1981).

An important point which was neglected in previous studies of Yelle (2004) and Tian et al. (2005) is the fact that for close-in gas giants, the Lagrangian L_1 point may be located somewhere in the expanded exosphere and may be even below the exobase (Lecavelier des Etangs et al., 2004; Jaritz et al., 2005; Erkaev et al., 2007; Lecavelier des Etangs, 2007). The Roche lobe is defined as a volume of space around a planet where its atmosphere is gravitationally bound to that planet. Because atmospheric particles at and beyond the Roche lobe can escape to space, Lecavelier des Etangs et al. (2004) argued that the Roche lobe can be seen as an equivalent to the exobase level. To be exact, there is a difference between the Roche lobe and the exobase, since at the Roche lobe the atmospheric particles can freely escape, whereas at the exobase level a critical temperature should be reached to allow blow-off to occur (at the L_1 point, the critical temperature is zero). For HD209458b the L1 point is at about $4.3R_{pl}$ (Erkaev et al., 2007) and the exobase is above or near the Roche lobe, hence, all particles reaching the L_1 point are lost automatically.

In order to study evolutionary aspects of extrasolar giant planet atmospheres, it is necessary to consider also the much higher XUV fluxes of younger stars (e.g., Ribas et al., 2005). Previous investigations of evolutionary effects of evaporating "Hot Jupiters"-like HD209458b by Lammer et al. (2003) and Baraffe et al. (2004) were based on the energy-limited approach of Watson et al. (1981), which have overestimated the thermal mass loss rates during evolutionary important early time periods. Lecavelier des Etangs (2007) proposed recently an approach for a fast estimation of the escape rates over the life time of the discovered "Hot Jupiters". His method is based on an energy diagram where the potential energy per unit mass of the planetary atmosphere is shown as a function of the stellar EUV energy flux absorbed in the upper atmosphere.

The escape rate is than obtained in a similar way, as suggested by Watson et al. (1981), as the ratio of the absorbed EUV energy flux integrated over the exoplanet to the potential energy of a unit mass of the atmosphere. Lecavelier des Etangs (2007) found a region, as a function of planetary and stellar parameters, in which a hydrogen-rich "Hot Jupiter" may evaporate in less than 5 Gyr. So far all known exoplanets were discovered outside this region.

In contrast to the previous studies which focused on evolutionary aspects of "Hot Jupiters" by Lammer et al. (2003), Baraffe et al. (2004) and Lecavelier des Etangs (2007), this study has the aim to investigate the difference between the mass loss calculations arising from the use of the simplified energy-limited methods, and a detailed 1-D time-dependent hydrodynamic model developed in this study which solves hydrodynamic equations numerically for HD209458b over the planet's history for XUV fluxes between 1 and 100 times that of the present Sun. In Section 2 and in the Appendix a description of the numerical method used in our study is given. The expected XUV flux behavior of HD209458b's host star at present and during the star life time is discussed in Section 3. In Section 4 we apply our model to HD209458b and calculate temperature, density, and velocity profiles, as well as hydrogen loss rates with and without IR cooling for the present XUV flux conditions of HD209458b's host star and consider the conditions that blow-off for "Hot Jupiters" can occur. After comparing our results with different models and taking into account observational limitations we calculate the hydrogen loss rate from HD209458b over the planet's life time considering the evolution of the host star XUV flux in Section 5. The model results are compared to previous evolution studies based on energy-limited loss estimations by Lammer et al. (2003), Baraffe et al. (2004), and Lecavelier des Etangs (2007). For investigating the atmospheric instability of "Hot Jupiters" at closer orbital distances we study the thermal loss rates from a HD209458b-like exoplanet at closer orbital distance of 0.02 AU. Finally, in Section 6 we discuss the implications of our results for close-in exoplanets which are expected to be discovered by the CoRoT space observatory during the near future.

2. Model description

2.1. Solution of the hydrodynamic equations

We model the hydrodynamic conditions for a hydrogen-rich atmosphere of "Hot Jupiters" by applying the set of the 1-D fluid equations for mass, momentum, and energy conservation in spherical coordinates

$$\frac{\partial n}{\partial t}+\frac{1}{r^2}\frac{\partial nvr^2}{\partial r}=0,$$

$$n\frac{\partial v}{\partial t}+nv\frac{\partial v}{\partial r}+\frac{1}{m}\frac{\partial p}{\partial r}=nF_{\mathrm{grav}},$$

$$nm\left(\frac{\partial E}{\partial t}+v\frac{\partial E}{\partial r}\right)=q-p\frac{1}{r^2}\frac{\partial r^2 v}{\partial r}+\frac{1}{r^2}\frac{\partial}{\partial r}\left(r^2\chi\frac{\partial T}{\partial r}\right), \quad (1)$$

where

$$p=nkT, \quad E=\frac{1}{\gamma-1}\frac{p}{nm}. \quad (2)$$

Here, n refers to the particle number density, v is the velocity of the fluid, m is the mass of a hydrogen atom, p is the thermal pressure, E is the total energy density, q is the XUV volume heating rate, T is the temperature of the atmospheric gas, k is the Boltzmann constant, γ is the adiabatic index, and χ is the heat conductance. Also included are gravitational effects, referred to as Roche lobe effects by taking

$$F_{\mathrm{grav}}=-\frac{GM_{\mathrm{pl}}}{r^2}+\frac{GM_{\mathrm{st}}}{(d-r)^2}-\frac{G(M_{\mathrm{st}}-M_{\mathrm{pl}})}{d^3}(s-r), \quad (3)$$

where G is the gravitational constant, M_{pl} is the planetary mass, M_{st} is the stellar mass, d is the orbital distance of the planet, and s is distance of the center of mass of the system from the planets center. A detailed description of the numerical method which we use for solving the hydrodynamic equations is given in the Appendix.

2.2. X-ray and EUV heating of the thermosphere

Below we establish a functional dependence between the XUV volume heating rate q and distance r, which we model by the following two integrals:

$$q(r)=\eta\tilde{n}q_{\max}s(r)\exp\left[-\kappa\int_1^r s(r')\,\mathrm{d}r'\right],$$

$$s(r)=\exp\left[\alpha\int_\infty^r n(r')\,\mathrm{d}r'\right], \quad (4)$$

where η is the heating efficiency which is defined as the ratio of the net heating rate to the rate of stellar energy absorption. In the present stage of our investigations we introduce an idealized heating function. The stellar XUV radiation intensity J decreases towards the exoplanet due to absorption in the thermosphere, which results in dissociation and ionization and, hence, in heating of the upper atmosphere

$$\frac{\mathrm{d}J}{\mathrm{d}r}=\sigma n^* J, \quad (5)$$

where σ is the ionization cross section and n^* is the total density of the neutral gas. By integrating Eq. (5), one obtains

$$J=J_\infty\exp\left(\alpha\int_\infty^{\tilde{r}}\tilde{n}^*\,\mathrm{d}\tilde{r}\right), \quad (6)$$

where $\alpha=\sigma n_0 r_0$ and $\tilde{r}$ and $\tilde{n}^*$ refer to normalized quantities. The neutral particle flux as a decreasing function of distance can be determined by the following

equation:

$$\mathrm{div}(n^*\mathbf{v}) = -\frac{Jn^*\sigma}{E_i}, \tag{7}$$

where E_i is the average energy of the XUV photons. From the equation of conservation $\mathrm{div}(n\mathbf{v}) = 0$ for the total number density n in the case of the radial flow, we obtain an equation for the ratio between the ion density and the total number density

$$\tilde{v}\frac{\mathrm{d}}{\mathrm{d}\tilde{r}}\left(\frac{n^*}{n}\right) = -\frac{J\sigma r_0}{c_s E_i}\left(\frac{n^*}{n}\right). \tag{8}$$

By taking the asymptotic of the velocity $\tilde{v}_\infty$ and by integrating Eq. (8) we find

$$\left(\frac{n^*}{n}\right) = \exp\left(-\kappa\int_1^{\tilde{r}}(J/J_\infty)\,\mathrm{d}\tilde{r}\right), \tag{9}$$

where $\kappa = J_\infty\sigma r_0/(E_i c_s \tilde{v}_\infty)$. By using (6) and (9) we find the source function for the XUV volume heating rate

$$q = \eta\sigma n^* J = \eta(\sigma n_0 J_\infty)\tilde{n}\left(\frac{J}{J_\infty}\right)\exp\left(-\kappa\int_1^{\tilde{r}}(J/J_\infty)\,\mathrm{d}\tilde{r}\right), \tag{10}$$

where $J/J_\infty = s(r) = \exp(\alpha\int_\infty^{\tilde{r}}\tilde{n}\,\mathrm{d}\tilde{r})$. By comparing (10) with (4) we define $q_{\max} = \sigma n_0 J_\infty$. We note that the obtained Chapman-like function for q represents an idealized shape of the XUV volume heating rate modeled by Yelle (2004) with a maximum $q_{\max}$ close to the visible radius in the thermosphere of the exoplanet and a sharp decline below and a smaller decrease above.

In order to study the effect of the heating efficiency on the temperature, velocity and density profiles and the corresponding hydrogen loss rate we use $\eta = 10\%$, 30%, and 60%, which covers the whole range of heating efficiencies found in the literature (Chassefière, 1996a; Yelle, 2004; Tian et al., 2005). Fig. 1 shows the heating rate in physical units for present day HD209458b and an IR cooling rate as used in our model. Since IR cooling processes take place in the lower thermosphere of HD209458b (Yelle, 2004), we introduce an IR cooling term q_{IR} in the heating function $q = q_{\mathrm{XUV}} - q_{\mathrm{IR}}$, where q_{XUV} represents the XUV heating term. Because at the present stage our model does not include ion and neutral chemistry, the cooling term q_{IR} is chosen in such a way so that the effective XUV volume heating rate corresponds to the expected "Hot Jupiter" neutral and ion hydrogen chemistry modeled by Yelle (2004).

3. The evolution of stellar activity and HD209458

Stellar activity decreases by orders of magnitudes during the stellar life time. The main parameter that affects the stellar activity is the rotation, one of the crucial ingredient of the stellar dynamo. In turn, the coronal properties affect the angular momentum evolution of stars and therefore the dynamo efficiency producing a feedback process with a tight interplay between the properties of the stellar interiors and those of the outer atmospheric layers.

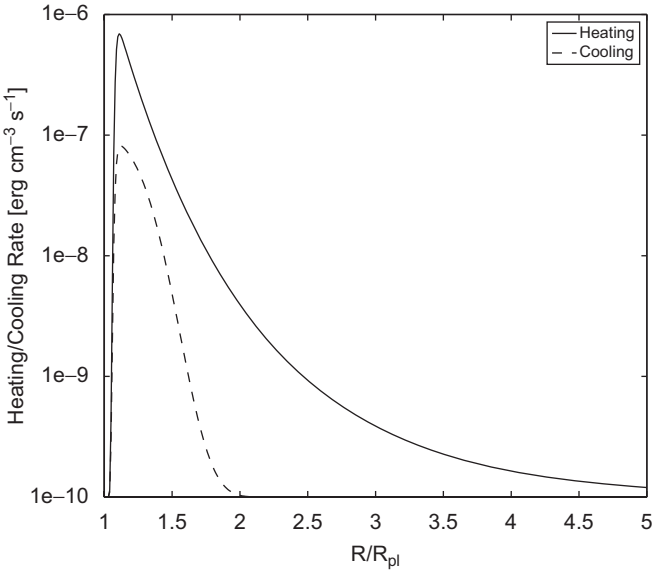

Fig. 1. Heating rate for the HD209458b present day thermosphere (solid line). The dashed line shows the cooling rate representing IR cooling.

The detailed history of rotational and activity evolution of a given star depends on the rotational velocity with which the star reaches the zero age main sequence (ZAMS). From observations of young open clusters we know that stars of a given mass just arrived on the ZAMS may have very different rotational periods (e.g., Bouvier et al., 1997), with $1M_\odot$ stars that may have periods of several days or of few hours. The specific value likely depends on the time when the circumstellar disk dissipates, since it regulates the angular momentum evolution during the premain sequence phase when the star is contracting. As a result of that a star that dissipates early its disk, may spin up during the contraction, reaching the ZAMS with fast rotation, while a star with a long living disk maintains a low rotation rate even during its contraction phase and will reach the ZAMS with a slow rotation rate.

Given the dependence of activity on rotation, stars on the ZAMS will present a broad distribution of activity levels. This broad distribution is particularly evident in X-ray bandpass, where it has been possible to derive luminosity distributions for stars of same mass and same age using stellar samples from open clusters. For example, dG stars in α Per (age $\sim$50 Myr) may have X-ray luminosity as low as $10^{29}\,\mathrm{erg\,s^{-1}}$ or much higher at $\log L_x \sim 3\times10^{30}\,\mathrm{erg\,s^{-1}}$ (Randich et al., 1996), dG stars of Pleiades (age $\sim$100 Myr) have X-ray luminisoty in the range of $4\times10^{28}-3\times10^{30}\,\mathrm{erg\,s^{-1}}$ (Stauffer et al., 1994; Micela et al., 1996). A broad X-ray luminosity range is present even at 1 Gyr as derived from Hyades cluster (Stern et al., 1995), and an even larger distribution has been determined for nearby stars that are dominated by stars of a few Gyr (Schmitt and Liefke, 2004). Furthermore it should be considered that, at least at the solar age, one

order of magnitude of variation is observed in X-ray bandpass during the solar cycle.

From all the above, it is clear that is very difficult, if not impossible, to reconstruct the "detailed" past history of the XUV flux of a specific star. Because, planetary migration is expected to occur also very early (e.g., Lin et al., 1996; Ward, 1997; Trilling et al., 1998; Burrows et al., 2000; Alibert et al., 2004; Rice and Armitage, 2005) one can assume that "Hot Jupiters" were exposed to much higher XUV radiation in their early evolutionary epochs. Because the host star of HD209458b is a solar-like G-type star we assume an average activity evolution derived from the project of *The Sun in time* (see, for example, Ribas et al., 2005 and references therein) that it is based on a sample of individual field solar proxies. Observations of young solar-like stars in this project indicate that the stellar XUV flux of Sun-like G-type stars 2.5 and 3.5 Gyr ago was about 3 and 6 times higher, respectively, than today and that the high-energy flux of the young solar-like stars after they arrived at the ZAMS was larger up to a factor of 100 (Ribas et al., 2005). The evolution of the XUV flux is calculated from the scaling law (Baraffe et al., 2004; Ribas et al., 2005)

$$F_{\mathrm{XUV}} = 6.13 t^{-1.19} f_{\mathrm{XUV}} \quad \text{for} \quad t \geqslant 0.1\,\mathrm{Gyr}, \tag{11}$$

where t is the age of the system in Gyr, while $f_{\mathrm{XUV}} = 420\,\mathrm{erg\,cm^{-2}\,s^{-1}}$ is scaled from the value given in Baraffe et al. (2004) to the orbit of HD209458b. The results should be considered as the behavior of an average G-type star. A complete derivation of the expected distribution of planetary losses taking into account the evolution of the complete X-ray luminosity distribution which are much higher will be deferred to a later work.

The present activity level of HD209458 can be estimated from an existing X-ray observation made with XMM/Newton observatory. Indeed the pre-release of the second version of the XMM/Newton Serendipitous Catalog (http://xmm.vilspa.esa.es/external/xmm_data_acc/xsa/index.shtml) reports an X-ray source at the stellar position with a count rate of $3.3 \times 10^{-3}\,\mathrm{cts\,s^{-1}}$. Assuming a hydrogen column $N_{\mathrm{H}} = 10^{19}\,\mathrm{cm^{-2}}$, a coronal temperature of $T = 3 \times 10^{6}\,\mathrm{K}$ and a distance of 47 pc we derive $L_x = 1.1 \times 10^{27}\,\mathrm{erg\,s^{-1}}$. Such luminosity is comparable with that of the present Sun during a moderately quiet phase and falls in the lower quartile of the X-ray luminosity distribution observed for the nearby solar-like stars (Schmitt, 1997).

4. Modeling of hydrogen loss rates for HD209458b

4.1. Velocity, density, and temperature profiles and their comparison with different models

For studying the effect of thermal evaporation during the history of HD209458b we apply our model first to the present stellar condition and observations so that the results can be compared to previous studies of other authors. HD209458b orbits at about 0.045 AU a 4 Gyr old solar-like G-type star. This "Hot Jupiter" has a planetary mass $M_{\mathrm{pl}} = 0.69 M_{\mathrm{Jup}}$ (Laughlin et al., 2005) and a visual radius $r_{\mathrm{pl}} \sim 1.32 r_{\mathrm{Jup}}$ (Knutson et al., 2007; Ballester et al., 2007). The XUV flux at 0.045 AU at present time is about 500 times larger compared with that on Earth at 1 AU.

The upper panel of Fig. 2 shows the flow velocity and number density for the present time XUV radiation value for η is 10% and 60% without (solid lines) and with (dashed lines) IR cooling. The corresponding flow velocity at the L_1 point for high and low η is in the order of about $7\,\mathrm{km\,s^{-1}}$. Assuming a hydrogen density at the lower boundary of the thermosphere $n_0 = 3 \times 10^{14}\,\mathrm{cm^{-3}}$ we obtain the number density profile as a function of distance for present day HD209458b shown in the middle panel of Fig. 2. By using this initial condition we achieve a density of about $10^{7}\,\mathrm{cm^{-3}}$ at $3.0 R_{\mathrm{pl}}$ and at the L_1 point, which is located at about $4.3 R_{\mathrm{pl}}$, a density of about $10^{6}\,\mathrm{cm^{-3}}$($\eta = 60\%$). As one can see in Fig. 2, if we use a lower heating efficiency ($\eta = 10\%$) we obtain slightly lower densities at the similar distances. The obtained values are in agreement with the observations of Vidal-Madjar et al. (2003, 2004). By comparing our obtained number densities with the neutral hydrogen density obtained by Yelle (2004) at $3 R_{\mathrm{pl}}$ one can see that our value is an order of magnitude higher but is in agreement with his total atomic hydrogen ($\mathrm{H} + \mathrm{H}^{+}$) density $n_{\mathrm{H+H^+}}$ of $\sim 10^{7}\,\mathrm{cm^{-3}}$. The reason is that in Yelle (2004) most H is ionized at distances $> 1.7 R_{\mathrm{pl}}$. At closer distances the hydrogen density profiles are different because in the present stage our model, like this of Tian et al. (2005), contains no hydrogen photochemistry.

The bottom panel of Fig. 2 shows the temperature profiles for $\eta = 10\%$ and 60% without IR cooling (solid lines) and with IR-cooling (dashed lines). For the temperature at the lower thermospheric boundary we use a value of $T_0 = 1350\,\mathrm{K}$ (Iro et al., 2005). The maximum temperatures achieved are ranging between 5000 and 10,000 K, depending on the heating efficiency and whether cooling is considered or not. In principle, these values could be compared with the observation of hot H by Ballester et al. (2007), who observed a small 0.03% absorption by atomic hydrogen. Using the atmospheric density and temperature profiles taken from the Yelle (2004) model, Ballester et al. (2007) concluded that the absorption could be produced in a 5000 K hot and 1000 km thick layer, located at an altitude of 8500 km. From this estimate it follows that the hot hydrogen layer is located at a radial distance of $\sim 1.09 R_{\mathrm{pl}}$ where it would give origin to the observed Balmer continuum absorption. This conclusion depends directly on the chemistry of the planet lower atmosphere, that is not included in the present code, preventing us to directly compare our modeling results with the observation by Ballester et al. (2007). We note that a detailed study of hot hydrogen generation in the thermosphere of HD209458b and the inclusion of hydrogen chemistry is beyond the scope of this work.

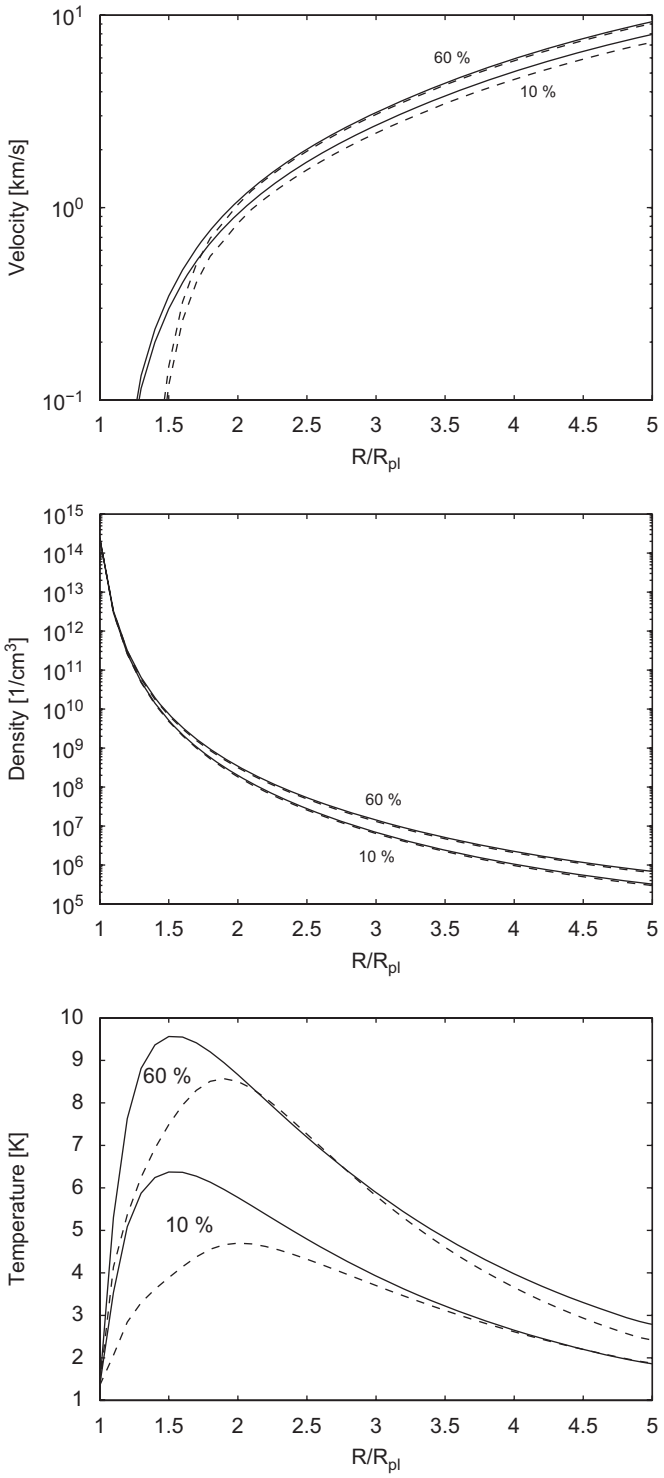

Fig. 2. Profiles for the flow velocity (upper panel), the density (middle panel), and the temperature for the present time XUV radiation level and the heating efficiency of 10% and 60%. The results are obtained with the IR-radiative cooling included (dashed lines) and without it (solid lines).

A comparison of the model results obtained in this study with the results of Yelle (2004) and Tian et al. (2005) for the present time stellar activity conditions for the planet HD 209458b is shown in the Fig. 3. The temperature profiles (the upper panel) and the velocity profiles (the lower panel)

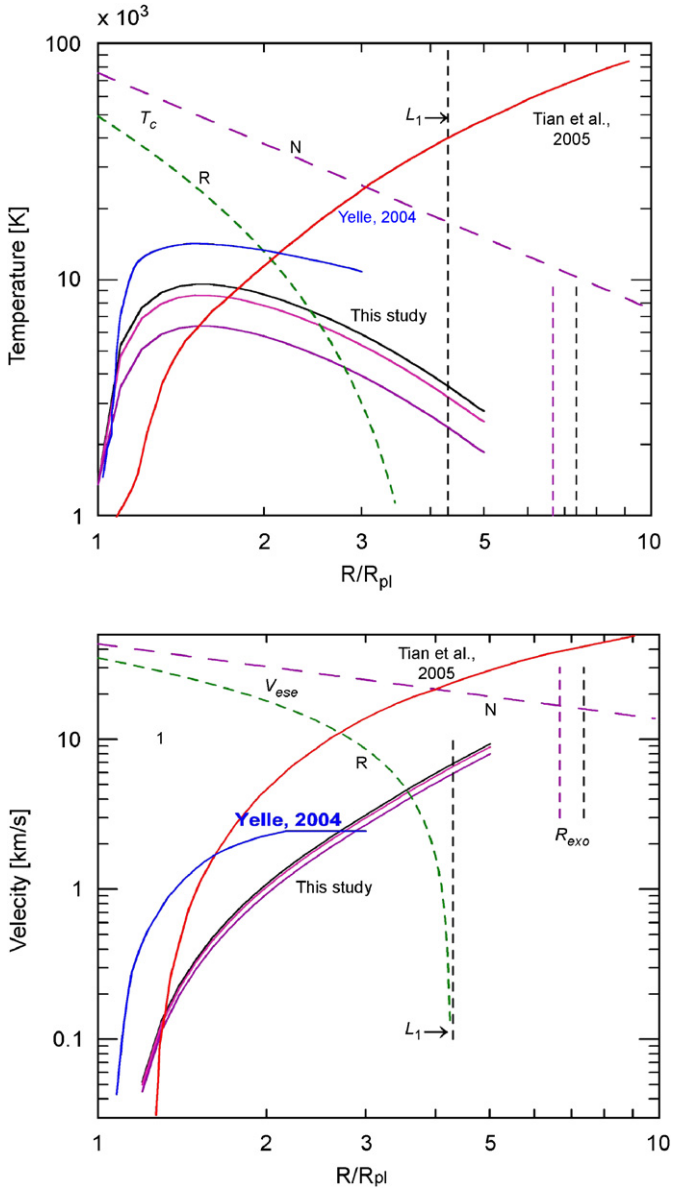

Fig. 3. Profiles for the temperature (upper panel) and the outflow velocity (lower panel) for the present time XUV radiation level obtained by Yelle (2004) and Tian et al. (2005) compared with the results of this study.

are presented by colored solid curves for all the three models in question as functions of the radial distance from the center of the planet. The three pairs of the temperature and velocity profiles calculated in this study for the three different XUV radiation heating efficiency values of $\eta = 10\%$, 30%, and 60% are shown in different colors. The critical temperature for the onset of blow-off, T_c and the escape velocity, V_{esc} profiles calculated for the Newtonian and Roche gravitational potentials of the planet according to Erkaev et al. (2007), are also displayed in Fig. 3 by the dashed curves. The L_1 point showing the Roche lobe boundary location and the exobase location, R_{exo} are also indicated in the figure by the vertical dashed lines. For the convenience of reference we shall denote hereafter our model, as P-2008 model, the reference model

of Yelle (2004, 2006), as Y-2004, and the Tian et al. (2005) model, as T-2005 model.

First, we compare our present time results with the Y-2004 model. It can be seen from Fig. 3 that a general behavior of the Y-2004 and of our P-2008 model temperature profiles is quite similar. They both show a rapid increase with the radial distance above the lower boundary of the model up to the peak temperature at about $1.5R_{pl}$ and a decline in temperature above the peak distance. The velocity profile for the Y-2004 model, like that for the P-2008 model, also shows a rapid increase above the lower boundary up to a distance of about $1.5R_{pl}$. Thus, we may conclude from this that both models are generically akin.

However, although our model and the Y-2004 model look basically similar, there are a few important differences between them, mostly in the details of the atmospheric structure they predict. First of all, the Y-2004 model yields notably higher maximum temperature. And, in spite of this, the temperatures of this model are well below the critical temperature, T_c for the onset of blow-off from the upper thermosphere of the planet. This follows from the high Newtonian gravitational potential barrier assumed at the upper boundary in this model. As a result, in the Y-2004 model only gas-kinetic evaporation is possible at the relatively slow subsonic atmospheric outflow velocities from the exobase level.

In contrast, although the temperatures predicted by our model for the heating efficiency in the range from 10% to 60% are notably lower than in the Y-2004 model, they are well above the critical temperature near the Roche lobe boundary, which results from the effect of the stellar tidal forces which are acting on the planetary atmosphere and are included in our model. As a consequence, our model predicts a hydrodynamic regime of atmospheric escape, that is blow-off, with a supersonic velocity above the Roche lobe at considerably lower temperatures than in the Y-2004 model.

When we compare our present time model results with those of the T-2005 model, one may note the high temperature achieved in that model, which reaches a maximum value close to 100,000 K near the upper boundary at $10R_{pl}$. This high temperature which is monotonously growing from the lower boundary, could be maintained in the tenuous upper atmosphere which experiences strong adiabatic cooling due to the expanding supersonic outflow, only if high energy deposition rate were assumed to heat the upper atmosphere of the planet above its Roche lobe. Also, very high velocity at distances above $\sim 2R_{pl}$ predicted by the T-2005 model which is about 5 times higher than in both Y-2004 and our model, indicates that the radiative heating of the upper atmosphere in the T-2005 model should be higher than in both Y-2004 and P-2008 models (see also Fig. 4).

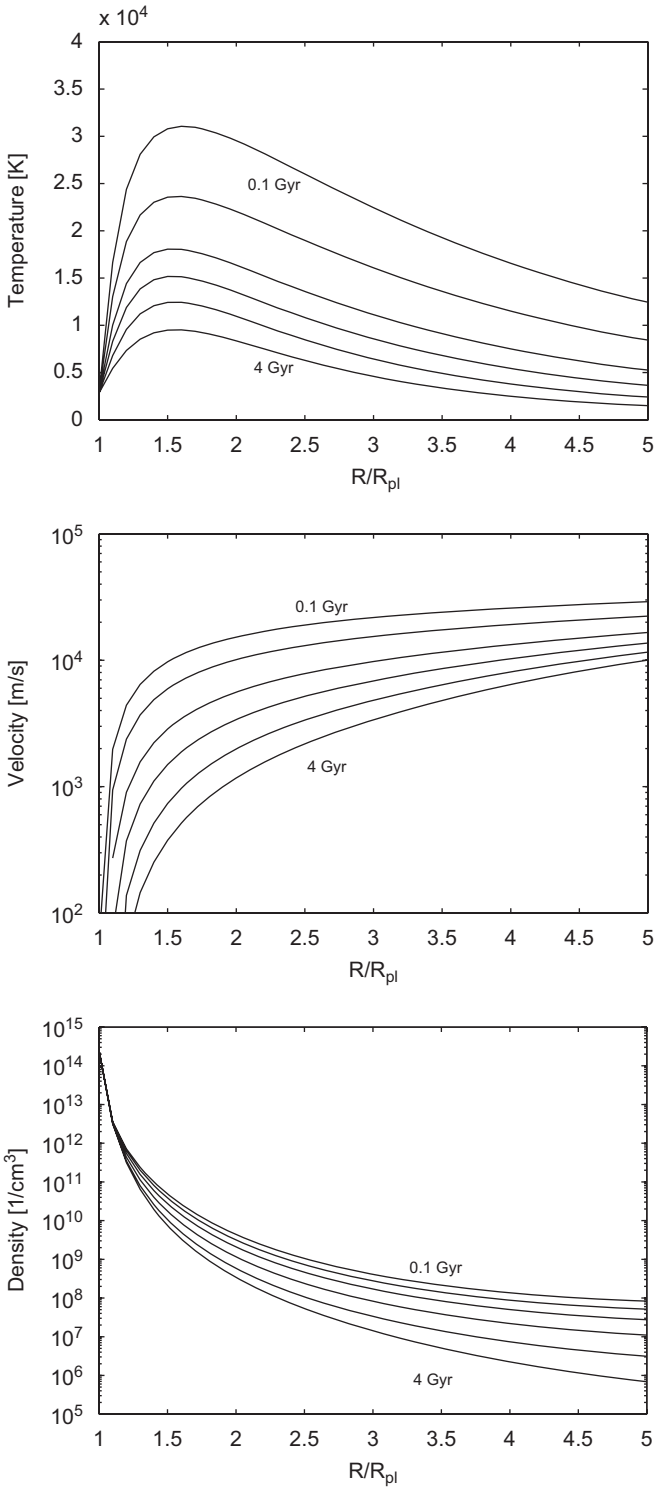

Fig. 4. Profiles for the temperature (upper panel), the flow velocity (middle panel), and the density (lower panel). The profiles represent different XUV radiation levels corresponding to 4, 2, 1, 0.5, 0.2, and 0.1 Gyr.

4.2. Present day thermal loss rates

We calculated the mass loss rate of HD209458b at the Roche lobe boundary, since above it no return to the atmosphere for all particle reaching this distance is possible. By using a high heating efficiency $\eta = 60\%$, our calculation yield a mass loss rate for HD209458b of about $3.5 \times 10^{10}\,\mathrm{g\,s^{-1}}$, which is higher than the loss rate of about $10^{10}\,\mathrm{g\,s^{-1}}$ estimated from the observations of Vidal-Madjar

Table 1
Loss rates in $g\,s^{-1}$ for different ages of the system (and corresponding XUV fluxes in $erg\,cm^{-2}\,s^{-1}$) using the hydrodynamic model and $\eta = 60\%$, 30%, and 10%, and the energy-limited approach (Erkaev et al., 2007) at an orbital distance of 0.045 AU

t (Gyr) (XUV flux ($erg\,cm^{-2}\,s^{-1}$))	4 (494)	2 (1127)	1 (2573)	0.5 (5871)	0.2 (17467)	0.1 (39852)	Total
HD model $\eta = 60\%$	3.5×10^{10}	1.2×10^{11}	4×10^{11}	9.2×10^{11}	3×10^{12}	6.2×10^{12}	5.7×10^{28} (4.4%)
$\eta = 30\%$	2.5×10^{10}	7.3×10^{10}	2.6×10^{11}	6.6×10^{11}	2×10^{12}	4.3×10^{12}	3.8×10^{28} (2.9%)
$\eta = 10\%$	1.3×10^{10}	4×10^{10}	1.6×10^{11}	4.6×10^{11}	1.2×10^{12}	2.4×10^{12}	2.3×10^{28} (1.8%)
Energy limited	1.4×10^{11}	3.3×10^{11}	7.6×10^{11}	1.6×10^{12}	5×10^{12}	1.2×10^{13}	1.1×10^{29} (8.4%)

et al. (2003). If we apply the IR cooling in our mass loss calculations, we find only slightly reduced escape rates. The cooling term changes the maximum temperature, but it does not significantly influence the other hydrodynamic quantities.

Our calculated total loss rate with $\eta = 60\%$ for the present time stellar activity conditions is in the range of the loss rates calculated by Yelle (2006) and Tian et al. (2005). One can see in Table 1 (4 Gyr case) calculated loss rates for lower heating efficiencies $\eta =$ of 30% and 10%. We find that in the case of lower heating efficiencies our model gives mass loss rates of about $2.5 \times 10^{10}\,g\,s^{-1}$ and $1.3 \times 10^{10}\,g\,s^{-1}$, respectively. By using the energy-limited escape as given by Erkaev et al. (2007), the loss rate would be $1.4 \times 10^{11}\,g\,s^{-1}$, slightly higher than the estimations of Lecavelier des Etangs (2007) who applied also an energy-limited approach with a 100% heating efficiency.

Another uncertain quantity is the neutral hydrogen number density in the lower thermosphere n_0, which is assumed to be $3 \times 10^{14}\,cm^{-3}$ in our reference case. If we assume it to be one order less, $n_0 = 3 \times 10^{13}\,cm^{-3}$, the loss rate is reduced from 3.5×10^{10} to $2 \times 10^{10}\,g\,s^{-1}$, while an increase of n_0 by one order of magnitude gives a loss rate $8 \times 10^{11}\,g\,s^{-1}$. Thus, changes of the homopause density can significantly change the results of the calculations by about a factor of 2 in both directions. After validating our model for the present mass loss conditions of HD209458b we investigate the evolution of the radiation environment of the planets host star, so that we can apply our model for mass loss calculations over HD209458b's history.

5. Thermal mass loss over the history of HD209458b

5.1. Early history thermal loss rates

For studying the loss rates of HD209458b over evolutionary time periods, we varied the volume heating rate q related to the evolving XUV flux of the host star, which could have been about 100 times larger after its arrival to the ZAMS than the present value (see Section 3; and Ribas et al., 2005). Fig. 5 shows our model results for $\eta = 60\%$ for density, temperature, and velocity profiles as a function of distance normalized to the planetary radii for ages of HD209458b's host star ranging from 0.1 to 4 Gyr. As expected, the values for all hydrodynamic quantities increase with decreasing age of the system. The density at

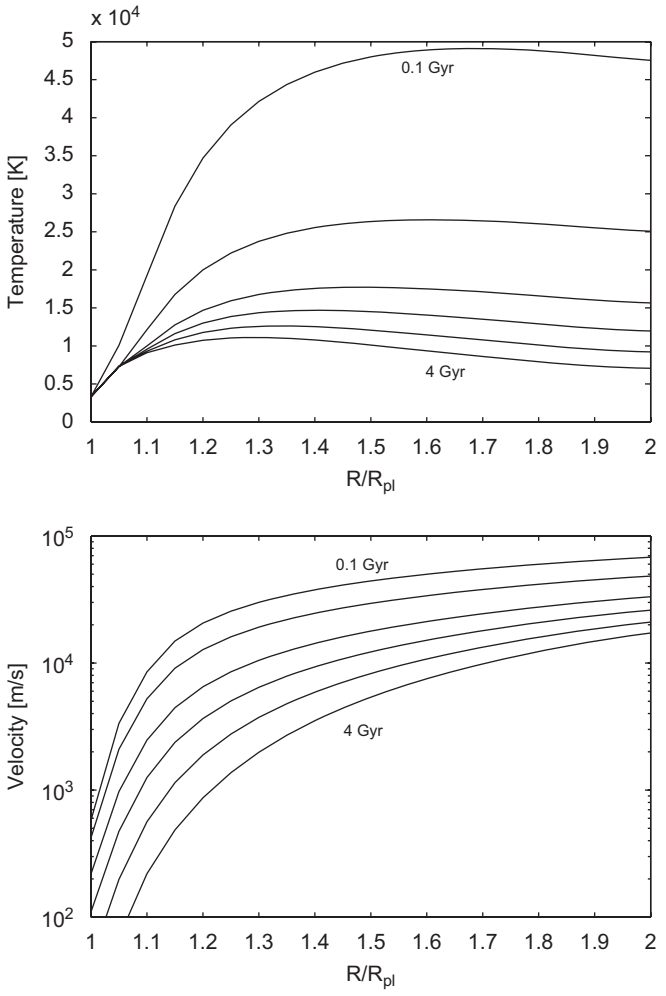

Fig. 5. Profiles for the temperature (upper panel), and the flow velocity (lower panel) for a heating efficiency of 60% of a HD209458b exoplanet orbiting at 0.02 AU. The profiles represent different XUV radiation levels corresponding to 4, 2, 1, 0.5, 0.2, and 0.1 Gyr.

the L_1 point increases from $10^6\,cm^{-3}$ at 4 Gyr to about $3 \times 10^7\,cm^{-3}$ at 1 Gyr and finally reaches about $10^8\,cm^{-3}$ at about 0.1 Gyr after the stars arrival at the ZAMS. The maximum temperature is changing from about 8000 K ($\eta =$ 30%) at 4 Gyr to about 15,000 K at 1 Gyr to more than 24,000 K at 0.1 Gyr. One might also notice that the radius where the maximum temperature is achieved is slightly increasing with increasing XUV flux, because the atmosphere is more expanded and thus the absorption radius

also increases leading to a slight shift of the location of the temperature maximum. The velocity close at the Roche lobe is changing from about $7\,km\,s^{-1}$ at 4 Gyr to about $25\,km\,s^{-1}$ at 0.1 Gyr.

The change in the mass loss rate is shown in Table 1. We compare the mass loss rate by using different heating efficiencies ($\eta = 60\%$, 30%, 10%) with the energy-limited loss rates ($\eta = 100\%$) obtained from the energy-limited approach of Erkaev et al. (2007). Furthermore, the influence of the IR cooling shown in Fig. 1 is also addressed for $\eta = 60\%$ cases. As already discussed above, the obtained mass loss rate rises for $\eta = 60\%$ from about $3.5 \times 10^{10}\,g\,s^{-1}$ at present time (4 Gyr) up to about $1.2 \times 10^{11}\,g\,s^{-1}$ 2 Gyr ago, while the energy-limited approach gives a loss rate of about $3.3 \times 10^{11}\,g\,s^{-1}$. At 0.5 Gyr the loss rate from the hydrodynamic model already reaches $9.2 \times 10^{11}\,g\,s^{-1}$, while the value is about a factor 2 higher by using the energy-limited approach. Finally, the atmospheric mass loss rate is more than $6 \times 10^{12}\,g\,s^{-1}$ at 0.1 Gyr after the star arrived at the ZAMS. We note that at this time period, the mass loss rate obtained with the energy-limited approach is about $10^{13}\,g\,s^{-1}$.

Integration of the hydrogen mass loss rate over HD209458b's life time of about 4 Gyr gives a total loss of about 5.7×10^{28} g for a high heating efficiency of $\eta = 60\%$, which is about 4.4% of the total mass of the present planet. This indicates that even for high XUV fluxes during the early stages of the planetary evolution and an assumed high heating efficiency, HD209458b did not lose a significant part of its mass due to thermal evaporation. For lower values for the heating efficiency, the loss rates are about 3.8×10^{28} g or about 2.9% of HD209458b's mass ($\eta = 30\%$), and 2.3×10^{27} g or 1.8% of HD209458b's mass ($\eta = 10\%$). The loss obtained by using the energy-limited approach is 1.1×10^{29} or 8.4% of the exoplanet's mass. By comparing these results with the loss rates obtained by Lammer et al. (2003) and Baraffe et al. (2004) one can see that these previous studies overestimated the thermal mass loss for HD209458b by at least one magnitude.

5.2. Atmospheric evolution of "Hot Jupiters" at very close orbital distances

However, it is also interesting to study the thermal evolution of gas giant atmospheres at even closer orbits, because they are affected by both, stronger XUV radiation and enhanced loss rates because of Roche lobe effects. Therefore, we put a planet with the same size and mass as HD209458b at an orbital distance of 0.02 AU around a solar-like G-type star and investigate the thermal mass loss over its history. At this close-in orbit, the effective temperature of the planet can be estimated as (Jaritz et al., 2005)

$$T_{\rm eff} = \left(\frac{3}{4}\tau + \frac{1}{2}\right)^{1/4} T_{\rm star}\left(\frac{1-A}{4}\right)^{1/4}\left(\frac{R_{\rm star}}{a}\right)^{1/2}, \qquad (12)$$

where τ is the optical depth, $T_{\rm star} = 6000$ K is the effective temperature of the star, $A = 0.52$ the albedo of the planet, while $R_{\rm star} = 1.01 R_{Sun}$ is the radius of the host star, and $a = 0.02$ AU is the orbital distance of the star. Using this equation, the effective temperature is $T_{\rm eff} = 2000$ K at the orbital distance of 0.02 AU. Additionally, we have to change the parameter accounting for the Roche lobe effects in the energy-limited approach. The position of the L_1 point in this system is located at $1.9 R_{\rm pl}$, which is already close to the visible radius of the planet.

Now we apply our hydrodynamic code and calculate loss rates for different ages of the system by using the maximum heating efficiency $\eta = 60\%$. Fig. 6 shows temperature and flow velocity profiles for different ages of the host star. It is obvious that the values are higher than for HD209458b at 0.045 AU. The temperature at 4 Gyr old planet is about 12,000 K, while it reaches 50,000 K at 0.1 Gyr after the host star arrived at the ZAMS. Also the flow velocity increases from $18\,km\,s^{-1}$ at 4 Gyr to $70\,km\,s^{-1}$ at 0.1 Gyr. At 4 Gyr, the atmospheric mass loss rate is about $2.6 \times 10^{11}\,g\,s^{-1}$, which is more than 7 times large than the mass loss rate at about 0.045 AU. For comparison, the mass loss rate without Roche lobe effects would be only $1.2 \times 10^{11}\,g\,s^{-1}$. Thus, as pointed out by Lecavelier des Etangs et al. (2004), Erkaev et al. (2007), and Lecavelier des Etangs (2007) one can see that at such close orbital distances, the Roche lobe already plays an important role.

If we proceed to early stages of the host star's evolution, a mass loss rate of about $2.2 \times 10^{13}\,g\,s^{-1}$ is found at 0.1 Gyr. An overview of the mass loss rates for a heating efficiency $\eta = 60\%$ is given in Table 2. If we integrate the loss over 4 Gyr, a total mass loss of about $3.6 \times 10^{29}\,g\,s^{-1}$ is

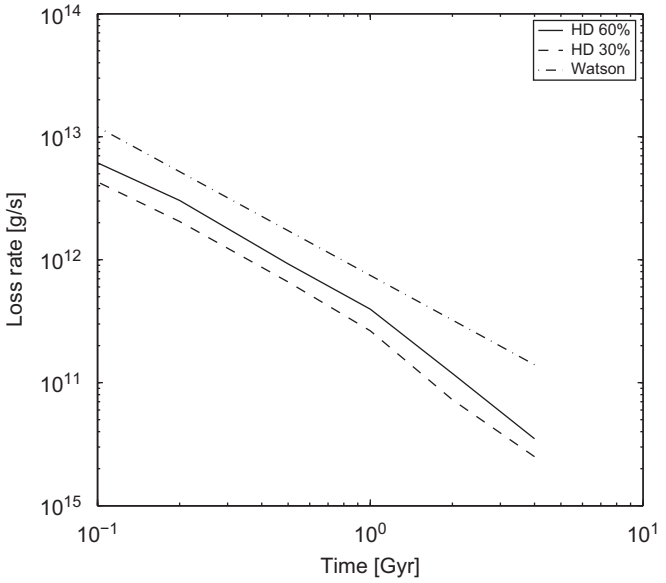

Fig. 6. Evolution of the mass loss from HD209458b orbiting with time from 0.1 to 4 Gyr at 0.045 AU. The solid line corresponds to the hydrogen mass loss rate for $\eta = 60\%$, the dashed line for $\eta = 30\%$, and the dashed-dotted line for the energy limited approximation ($\eta = 100\%$).

Table 2
Similar to Table 1 but for an HD209458b-like gas giant at an orbital distance of 0.02 AU

t (Gyr) (XUV flux (erg cm^{-2} s^{-1}))	4 (2502)	2 (5709)	1 (13026)	0.5 (29720)	0.2 (88429)	0.1 (201750)	Total
$\eta = 60\%$	2.6×10^{11}	9.4×10^{11}	3.2×10^{12}	8×10^{12}	1.5×10^{13}	2.2×10^{13}	3.6×10^{29} (27.5%)
Energy limited	1.6×10^{12}	3.7×10^{12}	8.6×10^{12}	2×10^{13}	5.7×10^{13}	1.3×10^{14}	1.2×10^{30} (91.5%)

found. This corresponds to about 27.5% of HD209458b's present mass and indicates that such close-in hydrogen-rich gas giants are significantly influenced by a combination of hydrodynamic and geometrical blow-off. The results for the energy-limited escape overestimate the hydrogen mass loss rate for the 0.1 Gyr case by a factor of 6.

Fig. 6 compares the hydrogen mass loss rates of HD209458b obtained by our hydrodynamic model calculations for $\eta = 60\%$ and 30% with the energy-limited approach ($\eta = 100\%$) as a function of time for orbital distances of 0.045 AU (upper panel). Our finding is in general agreement with the recent study of Lecavelier des Etangs (2007) who found a region where the "Hot Jupiters" may thermally evaporate at life times less than 5 Gyr. However, as one can see from Fig. 6 generalized methods which use an energy-limited approach overestimate the thermal mass loss rates. The overestimation of thermal evaporation rates by using energy-limited approaches and applied by Lammer et al. (2003) and Baraffe et al. (2004) may also explain the discrepancies between the mass function of observed "Hot Jupiters" and these previous evolutionary models. Hubbard et al. (2007a, b) recently presented calculations for the evolution and surviving of highly irradiated discovered exoplanets at orbital distances between 0.023 and 0057 AU by using a generalized scaling theory for mass loss including tidal truncation and found in agreement with our present results that the previous studies of Lammer et al. (2003) and Baraffe et al. (2004) overestimate the total mass loss and can therefore not reproduce the mass function of the observed "Hot Jupiters."

6. Contribution of CoRoT observations

For applying complex hydrodynamic codes which obtain reliably atmospheric mass loss rates to "Hot Jupiters" and lower mass exoplanets the size and mass of the planets as in the case of HD209458b has to be known. Unfortunately only a small sample of close-in exoplanets where the radius could be inferred by transit observations is available. For most of the more than 200 discovered exoplanets only the mass, including the uncertainty $\sin i$ is known from radial velocity measurements. However, the present situation will hopefully change after the successful launch of the CoRoT space observatory in December 27, 2006.

CoRoT will search continuously during 150 days at 6000–12,000 stars with high accuracy photometry for transiting exoplanets (Barge et al., 2006). With 5 long time observation runs and 3–4 short runs during a mission life time of about 2.5 yr the total target stars in the exoplanet search program of CoRoT will be about 30,000–60,000 on durations of about 150 days and about 20,000–40,000 on short time durations of about 20 days (Barge et al., 2006).

Due to the large number of target stars in CoRoTs observation channel, it is expected that CoRoT will discover most likely several hundred transiting "Hot Jupiters" from which the planetary size could be inferred (Barge et al., 2006). Radial velocity follow-ups of the discovered exoplanets will give us the possibility to determine the mass, density, and gravitational acceleration of the discovered exoplanets with high accuracy. Especially observations of smaller and lower-mass close-in exoplanets within orbital locations <0.02 AU, where all theoretical models expect extremely high thermal and non-thermal mass loss rates will enhance our understanding of atmospheric escape processes under extreme stellar conditions and remnants or cores of "gas giants". Although the extreme mass loss theory where strong mass loss triggers a rapid expansion of the planetary radius as presented by Baraffe et al. (2004) may be excluded for "Hot Jupiters" at orbital distances >0.02 AU, the discovered effect should be considered at very close orbital distances of about $\leqslant 0.02$ AU. Therefore, the planet sample enlarged with transit discoveries by CoRoT will help to improve the present statistic and understanding of "Hot Jupiters", their interaction with its host star and planet formation in general.

7. Conclusions

We apply a numerical 1-D time-dependent hydrodynamic model including tidal forces for studying hydrogen winds and corresponding atmospheric mass loss rates at HD209458b as a function of stellar XUV fluxes over evolutionary timescales. Depending on the assumed heating efficiency for hydrogen-rich Jovian-type thermospheres ($\eta = 10-60\%$), the maximum temperature obtained in our study at $1.5R_{pl}$ by neglecting IR cooling reaches about 5000–10,000 K.

Our obtained temperature at the Roche lobe distance of about $4.3R_{pl}$ is about 2500–3500 K, which is much less than the critical temperature of about 20,000 K required for blow-off in the case of the classical Newtonian gravitational potential. However, we found that the upper atmosphere of HD209458b experiences hydrodynamic blow-off at such low temperatures if one does not neglect

gravitational effects caused by the Roche lobe. By comparing our modeled temperature and velocity profiles with those obtained by Yelle (2004) and Tian et al. (2005) our results are in a better agreement with Yelle (2004) but in disagreement with Tian et al. (2005) results who obtained high temperatures of about 40,000 K at the L_1 point and even about 80,000 K at the exobase.

By using a heating efficiency η of 10%, 30%, and 60%, the corresponding present day thermal mass loss rate for HD209458b is found to be about 1.3×10^{10}, 2.5×10^{10}, and $3.5\times10^{10}\,\mathrm{g\,s^{-1}}$, respectively. Our result is consistent with the lower mass loss limit estimated from the HST-STIS Lyman-α observations of $\geqslant10^{10}\,\mathrm{g\,s^{-1}}$. The results obtained with the higher heating efficiencies are in agreement with the maximum mass loss rates of about 6×10^{10}, and $4.7\times10^{10}\,\mathrm{g\,s^{-1}}$ calculated by Tian et al. (2005), and Yelle (2006) but is significantly lower than the energy-limited mass loss rate of about $10^{12}\,\mathrm{g\,s^{-1}}$ which was estimated by Lammer et al. (2003) based on the assumptions of Watson et al. (1981).

By applying our model to higher XUV flux values as expected for young solar-like stars, we found that for a 100 times higher XUV exposure during the first 0.1 Gyr of the planets' evolution stage, mass loss rates from $2.4\times10^{12}\,\mathrm{g\,s^{-1}}$ for $\eta=10\%$ and $6.2\times10^{12}\,\mathrm{g\,s^{-1}}$ for $\eta=60\%$. The total integrated thermal mass loss over the history of HD209458b depends of the heating efficiency and XUV evolution of the planets' host star and is found to be in the order of about $2.3\times10^{27}-5.7\times10^{28}$ g, corresponding to about 1.8–4.4% of the mass of HD209458b. This value can vary by about a factor of 2 because of uncertainties in the homopause number density but is more than a magnitude lower than earlier estimates based on Watson's method (Lammer et al., 2003).

For investigating the efficiency on the orbit location to the thermal evaporation, we modeled the mass loss rates also for a closer orbit location of a HD209458b-like "Hot Jupiter" at about 0.02 AU and found that at an orbital location ~0.02 AU, HD209458b could have lost up to about 27.5% of its present mass due to higher stellar XUV radiation and Roche lobe effects.

Acknowledgements

T.P. acknowledges support by the Marie Curie Fellowship Contract no. MTKD-CT-2004-002769 of the project. The influence of stellar high radiation on planetary atmospheres", and the host institution INAF Osservatorio Astronomico di Palermo. T.P., D.L., H.L., and H.K.B. acknowledge support by the Austrian Academy of Sciences, "Verwaltungsstelle für Auslandsbeziehungen" and by the Russian Academy of Sciences (RAS) for supporting working visits to the Institute of Computational Modeling (ICM/RAS) in Krasnoyarsk and at the Polar Geophysical Institute (PGI/RAS) in Murmansk, Russian Federation. This work is supported by the Austrian "Fonds zur Förderung der wissenschaftlichen Forschung" (FWF) under Project P17099-N08 and P20341-N16, by Grants 04-05-64088, 03-05-20014_BNTS_a from the Russian Foundation of Basic Research. Also acknowledged is support by the "Österreichischer Austauschdienst" (ÖAD), which supported this work by the Project I.12/04 and I.2/04. Yu.N.K. and H.L. thank the Russian Foundation for the Basic Research, which partially supported this study as a joint Russian–Austrian Project no. 03-05-20003 "Solar-planetary relations and space weather". The authors also thank the Austrian Ministry for Science, Education and Culture (bm:bwk) and ASA for funding the CoRoT project. This study was supported by the International Space Science Institute (ISSI) and carried out in the frame of the ISSI Team "Evolution of Exoplanet Atomspheres and their Characterisation".

Appendix

Here we briefly discuss the numerical model used for solving the hydrodynamic equations (1). For computational convenience we introduce dimensionless quantities according to

$$r=r_0\tilde{r},\quad v=c_t\tilde{v},\quad t=r_0/c_t\tilde{t},\quad n=n_0\tilde{n},$$

$$T=\gamma T_0\tilde{T},\quad q=\frac{n_0mc_t^3}{r_0}\tilde{q},$$

where $c_t^2=\gamma RT_0$ denotes the sound velocity and subscript 0 refers to quantities at the visual radius r_{pl} of the planet. In the normalized units we can write the following system of equations:

$$\frac{\partial\tilde{n}}{\partial\tilde{t}}+\frac{2}{\tilde{r}}\tilde{n}\tilde{v}+\tilde{n}\frac{\partial\tilde{v}}{\partial\tilde{r}}+\tilde{v}\frac{\partial\tilde{n}}{\partial\tilde{r}}=0, \tag{13}$$

$$\tilde{n}\frac{\partial\tilde{v}}{\partial\tilde{t}}+\tilde{n}\tilde{v}\frac{\partial\tilde{v}}{\partial\tilde{r}}+\tilde{T}\frac{\partial\tilde{n}}{\partial\tilde{r}}+\tilde{n}\frac{\partial\tilde{T}}{\partial\tilde{r}}=-\beta_{pl}\tilde{n}\frac{1}{\tilde{r}^2}+\beta_{st}\tilde{n}\frac{1}{(\tilde{d}-\tilde{r})^2}-\beta_{plst}\tilde{n}\frac{M_{plst}\tilde{d}-\tilde{r}}{\tilde{d}^3}, \tag{14}$$

$$\frac{\partial\tilde{T}}{\partial\tilde{t}}+\tilde{v}\frac{\partial\tilde{T}}{\partial\tilde{r}}=(\gamma-1)\frac{\tilde{q}}{\tilde{n}}-(\gamma-1)\tilde{T}\frac{1}{\tilde{r}^2}\frac{\partial\tilde{r}^2\tilde{v}}{\partial\tilde{r}}, \tag{15}$$

where $\beta_{pl,st}=GM_{pl,st}/(r_{pl}c_t^2)$, $\beta_{plst}=G(M_{pl}+M_{st})/(r_{pl}c_t^2)$, and $M_{plst}=M_{st}/(M_{pl}+M_{st})$. Because we have only normalized quantities, we shall omit the superscript tilde hereafter.

Parker (1979) found analytic solutions of the problem in question, if one assumes a spatially constant temperature in the steady state (isothermal) case. Thus, the general behavior of the physical quantities is known, i.e. the density decreases as r^{-2} away from a planet, whereas the flow velocity of the fluid increases away from the planet and approaches asymptotically a constant value. We should note that in its present form, the system of Eqs. (13) is rather difficult to treat numerically due to the steep gradient of density, particularly in the immediate proximity of the planet. Therefore, we transform the

system of hydrodynamic equations into a form more suitable for numerical computations.

To overcome the problem of modeling steep density gradients, we introduce in the first step a new function $f = \ln n$, which is divided into two component parts $f = f_0 + f_1$. The function f_0 is taken to be a stationary component of the solution with a zero flow velocity and is assumed to satisfy the equations

$$\frac{\partial f_0}{\partial t} = 0, \quad \frac{\partial f_0}{\partial r} = -\frac{\beta_{\rm pl}}{r^2} + \frac{\beta_{\rm st}}{(d-r)^2} - \frac{\beta_{\rm plst}}{d^3}(M_{\rm plst}d - r). \quad (16)$$

Then the system of hydrodynamic equations reads

$$\frac{\partial f_1}{\partial t} + v\frac{\partial f_1}{\partial r} + \frac{\partial v}{\partial r} = -\frac{2v}{r} - v\frac{\partial f_0}{\partial r}, \quad (17)$$

$$\frac{\partial v}{\partial t} + v\frac{\partial v}{\partial r} + T\frac{\partial f_1}{\partial r} = -\frac{\partial T}{\partial r} + (1-T)\frac{\partial f_0}{\partial r}, \quad (18)$$

$$\frac{\partial T}{\partial t} + v\frac{\partial T}{\partial r} = (\gamma - 1)qe^{-(f_0+f_1)} - (\gamma - 1)T\frac{1}{r^2}\frac{\partial r^2 v}{\partial r}. \quad (19)$$

As a last step in transforming the system of equations to a form suitable for numerical computations, we consider the equations of mass and momentum conservation separately and rewrite them in their characteristic form. The equations of mass and momentum conservation are integrated together by applying Godunov's (1959) method. The evolution of the temperature is then determined via a leapfrog step. At the lower boundary which is assumed to be near the visible radius of the exoplanet, the temperature, velocity, and density are specified and kept constant in time. The system of the mass and momentum conservation equations is solved along the characteristics. The main advantage of this method is that along the characteristics the system of partial differential equations reduces to a system of ordinary differential equations. The method is applied until steady state solutions are achieved. The stability of the scheme is ensured by an appropriate choice of the time step as the Courant–Friedrichs–Lewy condition is checked at every successive step.

References

Alibert, Y., Mordasini, C., Benz, W., 2004. Migration and giant planet formation. Astron. Astrophys. 417, L25–L28.

Ballester, G.E., Sing, D.K., Herbert, F., 2007. The signature of hot hydrogen in the atmosphere of the extrasolar planet HD 209458b. Nature 445, 511–514.

Baraffe, I., Selsis, F., Chabrier, G., Barman, T.S., Allard, F., Hauschild, P.H., Lammer, H., 2004. The effect of evaporation on the evolution of close-in giant planets. Astron. Astrophys. 419, L13–L16.

Barge, P., Léger, A., Ollivier, M., Rouan, D., Schneider, J., Exoplanet CoRoT Team, 2006. Photometric search for transiting planets. In: Fridlund, M., Bagalin, A., Lochard, J., Conroy, L. (Eds.), The CoRoT Mission Pre-Launch Status—Stellar Seismology and Planet Finding, ESA SP-1306, pp. 83–92.

Bauer, S.J., 1971. Solar cycle variation of planetary exospheric temperatures. Nature 232, 101–102.

Becker, R.H., Clayton, R.N., Galimov, E.M., Lammer, H., Marthy, B., Pepin, R.O., Wieler, R., 2003. Isotopic signatures of volatile elements in terrestrial planets. Space Sci. Rev. 106, 377–410.

Bouvier, J., Forestini, M., Allain, S., 1997. The angular momentum evolution of low-mass stars. Astron. Astrophys. 326, 1023–1043.

Bundy, K.A., Marcy, G.W., 2000. A search for transit effects in spectra of 51 Pegasi and HD209458. ASP 112, 1421–1425.

Burrows, A., Guillot, T., Hubbard, W.B., Marby, M., Saumon, D., Lunine, J.I., Sudarsky, D., 2000. On the radii of close in giant planets. Astrophys. J. Lett. 534, L97–L100.

Charbonneau, D., Brown, T.M., Latham, D.W., Mayor, M., 2000. Detection of planetary transits across a Sun-like star. Astrophys. J. 529, L45–L48.

Charbonneau, D., Brown, T.M., Noyes, R.W., Gilland, R.L., 2002. Detection of an extra-solar planet atmosphere. Astrophys. J. 568, 377–384.

Chassefière, E., 1996a. Hydrodynamic escape of hydrogen from a hot water-rich atmosphere: the case of Venus. J. Geophys. Res. 101, 26039–26056.

Chassefière, E., 1996b. Hydrodynamic escape of oxygen from primitive atmospheres: application to the cases of Venus and Mars. Icarus 124, 537–552.

Erkaev, N.V., Kulikov, Yu.N., Lammer, H., Selsis, F., Langmayr, D., Jaritz, G.F., Biernat, H.K., 2007. Roche lobe effects on the atmospheric loss of "Hot Jupiters". Astron. Astrophys. 472, 329.

Godunov, S.K., 1959. A difference scheme for numerical solution of discontinuous solution of hydrodynamic equations. Mat. Sb. 47, 271–306 (translated US Joint Publ. Res. Service, JPRS 7226, 1969).

Gross, S.H., 1972. On the exospheric temperature of hydrogen-dominated planetary atmospheres. J. Atmos. Sci. 29, 214–218.

Henry, G.W., Marcy, G.W., Butler, R.P., Vogt, S.S., 2000. A transiting "51 Peg-like" planet. Astrophys. J. 529, L41–L44.

Hubbard, W.B., Hattori, M., Burrows, A., Hubeny, I., Sudarsky, D., 2007a. Effects of mass loss for highly irradiated giant planets. Icarus 187, 358–364.

Hubbard, W.B., Hattori, M., Burrows, A., Hubeny, I., 2007b. A mass function constraint on extrasolar giant planet evaporation rates. Astrophys. J. 658, L59–L62.

Hunten, D.M., 1973. The Escape of light gases from planetary atmospheres. J. Atmos. Sci. 30, 1481–1494.

Hunten, D.M., 1993. Atmospheric evolution of terrestrial planets. Science 259, 915–920.

Iro, N., Bézard, B., Guillot, T., 2005. A time-dependent radiative model of HD209458b. Astron. Astrophys. 436, 719–727.

Jaritz, G.F., Endler, S., Langmayr, D., Lammer, H., Grießmeier, J.-M., Erkaev, N.V., Biernat, H.K., 2005. Roche lobe effects on expanded upper atmospheres of short-periodic giant exoplanets. Astron. Astrophys. 439, 771–775.

Knutson, H., Charbonneau, D., Noyes, R.W., Brown, T.M., Gilliland, R.L., 2007. Using stellar limb-darkening to refine the properties of HD 209458b. Astrophys. J. 655, 564–575.

Lammer, H., Selsis, F., Ribas, I., Guinan, E.F., Bauer, S.J., 2003. Atmospheric loss of exoplanets resulting from stellar X-ray and extreme-ultraviolet heating. Astrophys. J. Lett. 598, L121–L124.

Laughlin, G., Marcy, G., Vogt, S., Fischer, D., Butler, P., 2005. Eccentricity of HD 209458b. Astrophys. J. 629, L121–L124.

Lecavelier des Etangs, A., 2007. A diagram to determine the evaporation status of extrasolar planets. Astron. Astrophys. 461, 1185–1193.

Lecavelier des Etangs, A., Vidal-Madjar, A., McConnell, J.C., Hébrard, G., 2004. Atmospheric escape from hot Jupiters. Astron. Astrophys. 418, L1–L4.

Lin, D.N.C., Bodenheimer, P., Richardson, D.C., 1996. Orbital migration of the planetary companion of 51 Pegasi to its present location. Nature 380, 606–607.

Micela, G., Sciortino, S., Kashyap, V., Harnden Jr., F.R., Rosner, R., 1996. ROSAT observations of the Pleiades. I. X-ray characteristics of a coeval stellar population. Astrophys. J. Suppl. 102, 75–103.

Moutou, C., Coustenis, A., Schneider, J., StGilles, R., Mayor, M., Queloz, D., Kaufer, A., 2001. Search for the spectroscopical signature of transiting HD209458 b's exosphere. Astron. Astrophys. 371, 260–266.

Parker, E.N., 1979. Comical Magnetic Fields: Their Origin and Their Activity. Clarendon Press, Oxford.

Pepin, R.O., 2000. On noble gas processing in the solar accretion disc. Space Sci. Rev. 92, 230–371.

Pepin, R.O., Porcelli, D., 2002. Origin of the noble gases in the terrestrial planets. Rev. Mineral. Geochem. 47, 191–246.

Randich, S., Schmitt, J.H.M.M., Prosser, C.F., Stauffer, J.R., 1996. The X-ray properties of the young open cluster around α Persei. Astron. Astrophys. 305, 785–805.

Rauer, H., Bockelée-Morvan, D., Coustenis, A.A., Guillot, T., Schneider, J., 2000. Search for an exosphere around 51 Pegasi B with ISO. Astron. Astrophys. 355, 573–580.

Ribas, I., Guinan, E.F., Güdel, M., Audard, M., 2005. Evolution of the solar activity over time and effects on planetary atmospheres I High-energy irradiances (1–1700 å). Astrophys. J. 622, 680–694.

Rice, W.K.M., Armitage, P.J., 2005. Quantifying orbital migration from exoplanet statistics and host metallicities. Astrophys. J. 630, 1107–1113.

Schmitt, J.H.M., 1997. Coronae on solar-like stars. Astron. Astrophys. 318, 215–230.

Schmitt, J.H.M.M., Liefke, C., 2004. NEXXUS: a comprehensive ROSAT survey of coronal X-ray emission among nearby solar-like stars. Astron. Astrophys. 417, 651–665.

Schneider, J., Rauer, H., Lasota, J.P., Bonazzola, S., Chassefière, E., 1998. The cometary tail of giant exoplanets at small orbital distances. In: Rebolo, R., Martin, E.L., Zapatero Osorio, M.R., (Eds.), Brown Dwarfs and Extrasolar Planets, ASP Conf. Series 134, Astronomical Society of the Pacific, Provo, Utah, pp. 241–244.

Stauffer, J.R., Caillault, J.-P., Gagne, M., Prosser, C.F., Hartmann, L.W., 1994. A deep imaging survey of the Pleiades with ROSAT. Astrophys. J. Suppl. 91, 625–657.

Stern, R.A., Schmitt, J.H.H.M., Kahabka, P.T., 1995. ROSAT all-sky survey observations of the hyades cluster. Astrophys. J. 448, 683–704.

Tian, F., Toon, O.B., Pavlov, A.A., De Sterck, 2005. Transonic hydrodynamic escape of hydrogen from extrasolar planetary atmospheres. Astrophys. J. 621, 1049–1060.

Trilling, D.E., Benz, W., Guillot, T., Lunine, J.I., Hubbard, W.B., Burrows, A., 1998. Orbital evolution and migration of giant planets: modeling extrasolar planets. Astrophys. J. 500, 428–439.

Vidal-Madjar, A., Lecavalier des Etangs, A., Désert, J.-M., Ballester, G.E., Ferlet, R., Hébrand, G., Mayor, M., 2003. An extended upper atmosphere around the extrasolar planet HD209458b. Nature 422, 143–146.

Vidal-Madjar, A., Désert, J.-M., Lecavelier des Etangs, A., Hébrard, G., Ballester, G.E., Ehrenreich, D., Ferlet, R., McConnell, J.C., Mayor, M., Parkinson, C.D., 2004. Detection of oxygen and carbon in the hydrodynamically escaping atmosphere of the extrasolar planet HD209458b. Astrophys. J. 604, L69–L72.

Ward, W.R., 1997. Protoplanetary migration by nebula tides. Icarus 126, 261–281.

Watson, A.J., Donahue, T.M., Walker, J.C.G., 1981. The dynamics of a rapidly escaping atmosphere: applications to the evolution of Earth and Venus. Icarus 48, 150–166.

Yelle, R., 2004. Aeronomy of extra-solar giant planets at small orbital distances. Icarus 170, 167–179.

Yelle, R., 2006. Corrigendum to Aeronomy of extra-solar giant planets at small orbital distances (Icarus 170 (2004) 167–179). Icarus 183, 508.

Zahnle, K., Kasting, J.F., Pollack, J.B., 1990. Mass fractionation of noble gases in diffusion-limited hydrodynamic hydrogen escape. Icarus 84, 502–527.

Zahnle, K.J., Kasting, J.F., 1986. Mass fractionation during transonic escape and implications for loss of water from Mars and Venus. Icarus 68, 462–480.